Acta Pharmaceutica Sinica B 2021;11(9):2685–2693

Chinese Pharmaceutical Association
Institute of Materia Medica, Chinese Academy of Medical Sciences

Acta Pharmaceutica Sinica B

www.elsevier.com/locate/apsb
www.sciencedirect.com

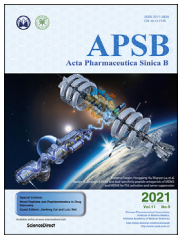

ORIGINAL ARTICLE

A novel ω-conotoxin Bu8 inhibiting N-type voltage-gated calcium channels displays potent analgesic activity

Jinqin Chen[a], Xinhong Liu[b,d], Shuo Yu[a], Jia Liu[a], Rongfang Chen[a], Yunxiao Zhang[c], Ling Jiang[b,*], Qiuyun Dai[a,*]

[a]*Beijing Institute of Biotechnology, Beijing 100071, China*
[b]*Key Laboratory of Magnetic Resonance in Biological System, State Key Laboratory of Magnetic Resonance and Atomic and Molecular Physics, Wuhan Center for Magnetic Resonance, Innovation Academy for Precision Measurement Science and Technology, Chinese Academy of Sciences, Wuhan 430071, China*
[c]*College of Life Science, Hunan Normal University, Changsha 410081, China*
[d]*University of Chinese Academy of Sciences, Beijing 100049, China*

Received 21 December 2020; received in revised form 13 February 2021; accepted 1 March 2021

KEY WORDS

N-type calcium ion channel;
ω-conotoxin;
Bu8;
Analgesic activity;
Structure–activity relationship

Abstract ω-Conotoxins inhibit N-type voltage-gated calcium ($Ca_V2.2$) channels and exhibit efficacy in attenuating neuropathic pain but have a low therapeutic index. Here, we synthesized and characterized a novel ω-conotoxin, Bu8 from *Conus bullatus*, which consists of 25 amino acid residues and three disulfide bridges. Bu8 selectively and potently inhibits depolarization-activated Ba^{2+} currents mediated by rat $Ca_V2.2$ expressed in HEK293T cells (IC_{50} = 89 nmol/L). Bu8 is two-fold more potent than ω-conotoxin MVIIA, a ω-conotoxin currently used for the treatment of severe chronic pain. It also displays potent analgesic activity in animal pain models of hot plate and acetic acid writhing but has fewer side effects on mouse motor function and lower toxicity in goldfish. Its lower side effects may be attributed to its faster binding rate and higher recovery ratios. The NMR structure demonstrates that Bu8 contains a small irregular triple β-strand. The structure–activity relationships of Bu8 Ala mutants and Bu8/MVIIA hybrid mutants demonstrate that the binding mode of $Ca_V2.2$ with the amino acid residues in loop 1 and loop 2 of Bu8 is different from that of MVIIA. This study characterizes a novel, more potent ω-conotoxin and provides new insights for designing $Ca_V2.2$ antagonists.

Abbreviations: DIEA, diisopropylethylamine; ESI-MS, electrospray ionization-mass spectroscopy; Fmoc, *N*-(9-fluorenyl)methyloxy-carbonyl; HBTU, 2-(1*H*-benzotriazol-1-yl)-1,1,3,3-tetramethyluronium hexafluorophosphate; HOBt, 1-hydroxybenzotriazole; IC_{50}, half-maximal inhibitory concentration; RP-HPLC, reversed phase high-performance liquid chromatography; TFA, trifluoroacetic acid.

*Corresponding authors. Tel: +86 10 66948897.
E-mail addresses: lingjiang@wipm.ac.cn (Ling Jiang), qy_dai@yahoo.com, daiqy@bmi.ac.cn (Qiuyun Dai).

Peer review under responsibility of Chinese Pharmaceutical Association and Institute of Materia Medica, Chinese Academy of Medical Sciences.

https://doi.org/10.1016/j.apsb.2021.03.001

1. Introduction

Conotoxins are active peptides derived from cone snail venoms[1,2]. They specifically target various ion channels (Na^+, K^+, and Ca^{2+} channels) and membrane receptors (nicotinic acetylcholine receptors (nAChR), *N*-methyl-D-aspartate receptor (NMDAR) and G protein-coupled receptors, etc.)[3−7]. ω-Conotoxins belong to a family of conotoxins and are usually composed of 25−40 amino acids folded with three disulfide bonds (C-C-CC-C-C)[5]. To date, 22 ω-conotoxins which inhibit L-($Ca_V1.1$), N-($Ca_V2.2$) and P/Q-type ($Ca_V2.1$) calcium channels have been characterized with several of these conotoxins specifically targeting $Ca_V2.2$[7−21]. $Ca_V2.2$ is highly expressed in superficial layers of the spinal cord and dorsal root ganglion neurons and modulates pain and other physiological signal processing[22−24]. Currently, one ω-conotoxin MVIIA (ziconotide) has been approved as an analgesic by the U.S. Food and Drug Administration (FDA)[25]. It selectively inhibits $Ca_V2.2$ and shows potent analgesic activity to chronic pain. We previously identified a new ω-conotoxin SO-3 with similar inhibitory activity to $Ca_V2.2$ and analgesic potency compared to MVIIA, but it shows lower side effects on motor function[17,26,27]. However, current $Ca_V2.2$ inhibitors still have apparent side effects because they also affect the normal physiological function of $Ca_V2.2$, such as motor functions[27]. In addition, selectivity of $Ca_V2.2$/$Ca_V2.1$ and reversibility also contribute to the side effects.

In order to discover new $Ca_V2.2$ inhibitors with higher potency and lower side effects, we synthesized a series of ω-conotoxins from several cone snails (*Conus achatinus*, *Conus bullatus* and *Conus catus*) and determined their potency to inhibit $Ca_V2.2$. We discovered that a new ω-conotoxin Bu8, whose amino acid sequence is derived from genes of *C. bullatus*[28] and significantly different from that of MVIIA. Importantly, Bu8 potently and selectively inhibited $Ca_V2.2$ with two-fold higher potency compared to MVIIA. Bu8 displayed a low inhibitory activity against $Ca_V2.1$, $Ca_V1.1$, sodium and potassium channels in rat DRG neurons. To probe the functional amino acids, Ala mutants of Bu8 were synthesized and evaluated. The analgesic activities of Bu8 were further assessed in mice using hot plate and acetic acid writhing pain models. The side effects of Bu8 were analyzed on mice motor function, and its toxicity on goldfish. The results show that Bu8 has higher or similar analgesic activity compared to MVIIA in the pain models mentioned above, and lower side effects. To analyze the reasons of lower side effects, the binding rates and the recovery ratios of Bu8 and MVIIA were compared. Furthermore, the NMR structure of Bu8 was determined and compared with MVIIA and SO-3. Based on the activity analyses of Ala mutants of Bu8 and Bu8/MVIIA hybrid mutants, we found that the binding mode of $Ca_V2.2$ with the amino acids in loop 1 and loop 2 of Bu8 are different from that of MVIIA. This study provides a novel ω-conotoxin with higher potency and new insights for designing $Ca_V2.2$ antagonists.

2. Results

2.1. Synthesis and characterization of Bu8 and its variants

After peptide folded in buffer at 4 °C for 24−48 h, HPLC analysis showed that all linear peptides folded into one major peak and several minor peaks. Fig. 1 shows a typical HPLC analysis (the analyses of aim products see Supporting Information Figs. S1−S15). Solutions containing folded products were concentrated in a preparative C18 column, eluted and lyophilized, and the aim product was purified and assessed with analytical C18 reverse-phase HPLC. The purity of all peptides was more than 95%. The results of mass spectrometry (micrOTOF-Q II mass spectrometer (Bruker, Bremen, Germany) showed that the peptides had the expected molecular weights (Table 1[26], Figs. S16−S30).

2.2. Circular dichroism (CD) spectroscopy

CD spectra of Bu8 and its variants shows a β-sheet conformation exists because positive Cotton effects around 245 nm and negative ones around 205 nm (Fig. 2) were observed. Compared to Bu8, S6A, T11A and T11L mutants exhibited a lower ellipticity, while other mutants had similar or higher ellipticity, suggesting that the β-sheet conformation contents are different among the peptides[29−31].

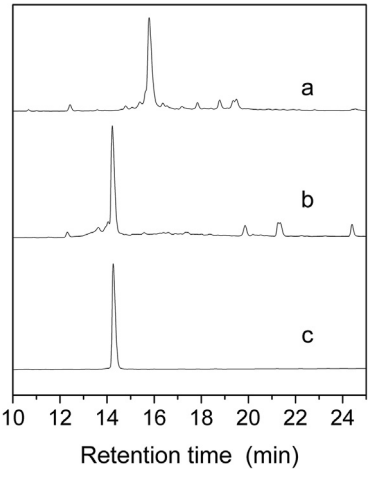

Figure 1 HPLC analyses of the folded products of linear Bu8. Spectra from top to bottom: (a) Linear peptide; (b) The folding products; (c) Purified Bu8. The crude linear peptides, folding products and pure peptide were analyzed using an Agilent Eclipse Plus C18 (5 μm, 250 mm × 4.6 mm). The elution gradient is as follows: 0−1 min, 5%−5% B; 1−25 min, 5%−35% B; 25−28 min, 35%−95% B (B is acetonitrile (0.1% TFA). The flow rate was 1 mL/min, λ = 214 nm.

2.3. NMR structure of Bu8

The structural statistics for Bu8 are given in Supporting Information Table S1. The ensemble of the 20-lowest energy structures and the ribbon representation are shown in Fig. 3A and B, respectively. Bu8 adopts a canonical globular scaffold (Fig. 3A), demonstrated as a inhibitory cysteine knot motif[7] marked by 3 disulfide bonds that is consistent for all ω-conotoxins in the all-crossing pattern of 1−4, 2−5, and 3−6, as shown in Fig. 3B. Bu8 also contains a small irregular triple β-strand, namely residues 6−8, 20−21, and 24−25. The disulfide bonds between Cys1 and Cys16 bring the N-terminal in close contact with the rigid β-sheet part of the structure, and the disulfide bonds between Cys15 and Cys25 does the same with the C-terminal. The disulfide bond between Cys8 and Cys20 additionally strengthens the triple-stranded β-sheet by interconnecting β-strand 1 and 2. Within the structure are two β-turns, characterized by a hydrogen bond between the carbonyl oxide of residue i and the amide hydrogen of residue i+3. One β-turn is between Lys 3 and Ser 6, the other between Arg21 and Lys24. For the first β-turn, the Gly5 on the i+2 position was also found to be absolutely conserved throughout this set of peptides. The type of the second turn may vary according to different residue types and in this case, it favors a tight β-turn due to the existence of the i+2 glycine. The whole peptide chain is commonly divided into loops 1−4 by recognizing the conserved cysteine distribution, C-(loop1)-C-(loop2) -CC-(loop3)-C-(loop4)-C. While loop1 and loop4 are shown to be rigid due to the formation of β-turns and β-strands, loop2 from Arg9 to Asp14 is less defined and serves as the binding site for voltage-gated calcium channels where important binding residues Arg10, Thr11, and Tyr13 reside.

2.4. Inhibition of $Ca_V2.2$-mediated currents by Bu8 and its mutants

The inhibitory activity of Bu8 and its mutants at $Ca_V2.2$ channels was determined in HEK293 cells expressing α1B, β3 and α2δ subunits. Representative traces of $Ca_V2.2$ depolarization-activated Ba^{2+} currents inhibited by 2 μmol/L Bu8 and MVIIA are shown in Fig. 4A and B. The concentration–response curves and the summary of IC_{50} values of MVIIA, Bu8 and its mutants are shown in Fig. 4 and Table 1. In the presence of extracellular solution containing 20 mmol/L Ba^{2+}, Bu8 potently inhibited $Ca_V2.2$ with an IC_{50} of 89 nmol/L, which is two-fold more potent than MVIIA (IC_{50} = 208 nmol/L). A lower IC_{50} value of Bu8 (14.4 nmol/L) was also obtained in the presence of 10 mmol/L Ba^{2+}, less than half of that of MVIIA (34.3 nmol/L, Supporting Information Fig. S31). Taking both the 'run-down' of $Ca_V2.2$ currents and recording convenience into account, the extracellular solution containing 20 mmol/L Ba^{2+} was used to determine the inhibitory activities of toxins.

When Ser6, Ser7, Ser12 and Asn22 were substituted with Ala, the IC_{50} values of Bu8[S6A], Bu8[S7A], Bu8[S12A] and Bu8[N22A] were 68, 98, 107 and 87 nmol/L, respectively, which corresponds to similar or lower potency compared to wild-type Bu8. However, the IC_{50} values of Bu8 mutants Bu8[R3A] (154 nmol/L), Bu8[R9A] (418 nmol/L) and Bu8[T11A] (793 nmol/L) were significantly higher compared to wild-type Bu8 (2, 4, and 9-fold, respectively). Together, these data suggest that Arg3, Arg9 and Thr11 are key functional amino acid residues, while Ser7, Ser12 and Asn22 are not as functionally important.

In order to compare the mechanisms of action of Bu8 and MVIIA, the Bu8/MVIIA hybrid mutants in loop1 and loop2 were selectively evaluated because the amino acid residues in loop3 and loop4 are the same except for Asn22, which is not a functional residue. After the replacement of Arg3, Arg9, Thr11, and Ser12 with the corresponding amino acids of MVIIA at the same positions (*i.e.*, Gly3, Ser9, Leu11 and Met12), the IC_{50} values of the resultant variants Bu8[R3G] (IC_{50} = 129 nmol/L), Bu8[R9S] (136 nmol/L), Bu8[S12M] (172 nmol/L) and Bu8[N22S] (95 nmol/L) were increased by 45%, 53%, 93%, and 7% compared to wild-type Bu8, respectively. On the other hand, one mutant, Bu8[T11L], showed a 26% increase in potency (IC_{50} = 68 nmol/L) compared to wild-type Bu8. These results suggest that the higher potency of Bu8 compared to MVIIA relies on 3 amino acids, while a 4th amino acid, T11, appears to counter-balance the other 3 amino acids a bit. The overall potency of Bu8 is twice that of MVIIA, which appears to result from not one single amino acid change, but from the combined effect of all 4 amino acids.

Our results also show that Bu8 blocks $Ca_V2.2$ more rapidly than MVIIA whereby at a concentration of 2 μmol/L, the onset of block of Bu8 is 2.33 min compared to 3.50 min for MVIIA

Table 1 Amino acid sequence and inhibitory activities of Bu8 and its variants with respect to $Ca_V2.2$.

No.	Name	Amino acid sequence	Theoretical MW (experimental, Da)[#]	IC_{50} (nmol/L, 95% confidence intervals)
Bu8	Bu8	**C**K**R**KG**SS**C**R**R**TS**YDC**C**TGSC**R**N**G**K**C***	2751.19(2752.11)	89 (85−93)
1	Bu8[R3A]	**C**K***A***KGSSC**R**RTSYDC**C**TGSC**R**NGK**C***	2666.13(2667.07)	154 (142−167)
2	Bu8[S6A]	**C**KRKG***A***SC**R**RTSYDC**C**TGSC**R**NGK**C***	2735.20(2736.11)	68 (63−73)
3	Bu8[S7A]	**C**KRKGS***A***C**R**RTSYDC**C**TGSC**R**NGK**C***	2735.20(2736.11)	98 (93−100)
4	Bu8[R9A]	**C**KRKGSSC***A***RTSYDC**C**TGSC**R**NGK**C***	2666.13(2667.07)	418 (391−447)
5	Bu8[T11A]	**C**KRKGSSC**R**R***A***SYDC**C**TGSC**R**NGK**C***	2721.18(2722.10)	793 (719−875)
6	Bu8[S12A]	**C**KRKGSSC**R**RT***A***YDC**C**TGSC**R**NGK**C***	2735.20(2736.13)	107 (98−116)
7	Bu8[N22A]	**C**KRKGSSC**R**RTSYDC**C**TGSC**R*A***GK**C***	2708.19(2709.12)	87 (81−93)
8	Bu8[R3G]	**C**K***G***KGSSC**R**RTSYDC**C**TGSC**R**NGK**C***	2652.11(2653.06)	129 (111−150)
9	Bu8[R9S]	**C**KRKGSSC***S***RTSYDC**C**TGSC**R**NGK**C***	2682.12(2683.06)	136 (126−147)
10	Bu8[T11L]	**C**KRKGSSC**R**R***L***SYDC**C**TGSC**R**NGK**C***	2763.23(2764.14)	68 (65−70)
11	Bu8[S12M]	**C**KRKGSSC**R**RT***M***YDC**C**TGSC**R**NGK**C***	2795.20(2796.12)	172 (145−204)
12	Bu8[N22S]	**C**KRKGSSC**R**RTSYDC**C**TGSC**R*S***GK**C***	2724.18(2725.11)	95 (90−100)
MVIIA	MVIIA	**C**K***G***KG***AK***C***S***R***LM***YDC**C**TGSC**R*S***GK**C***	2637.15(2638.07)	208 (180−239)
SO-3	SO-3	CKAAGKPCSRIAYNCCTGSCRSGKC*	2559.13(2560.28)	160 (100−220)[26]

*C-terminus is amidated; #M+H, isotopic; n = 3−6.

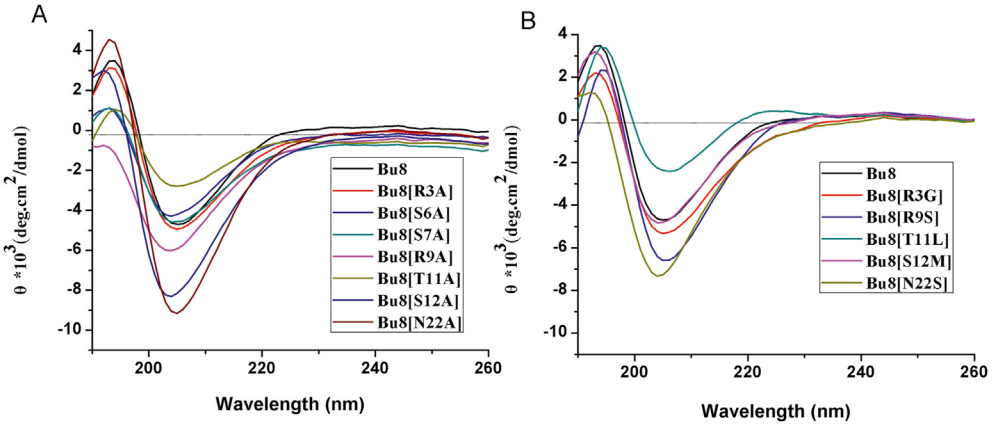

Figure 2 Circular dichroism spectra of Bu8 and its variants. (A) and (B), CD of the peptides in 0.01 mol/L PBS (pH = 7.2). $n = 3$.

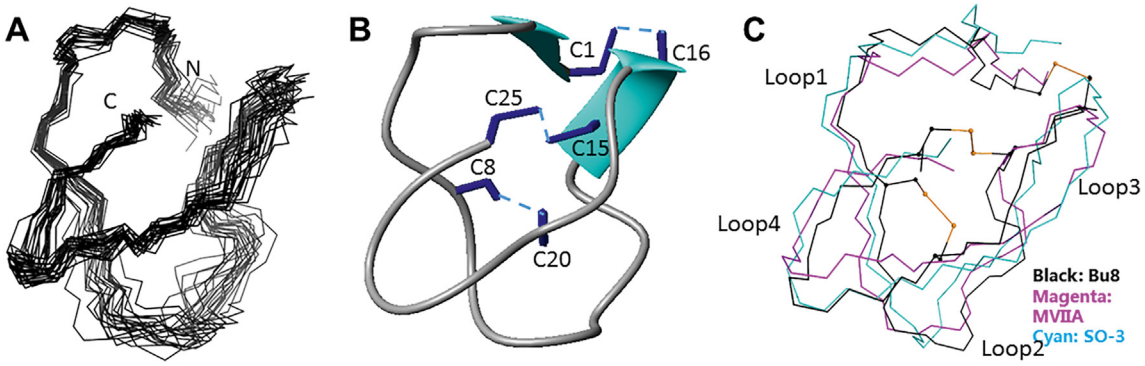

Figure 3 3D NMR solution structures of Bu8 and its comparisons with MVIIA and SO-3. (A) Superposition of 20 structures of Bu8 with the lowest energy, aligned with residues 2−7 and residues 19−24. The data were submitted to the BMRB database (ID: 36177) and the PDB database (ID 5ZNU). (B) Bu8 backbone with disulfide bonds (C1−C16, C8−C20, and C15−C25) and β-sheet structure. (C) Comparison of the backbone conformations of Bu8 (black), MVIIA (magenta), and SO-3 (cyan). The peptides are divided into loops 1−4, namely residues 2−7, 9−14, 17−19, and 21−24, respectively, interspaced by the cysteines. The toxins are aligned by backbone and the side chains of residues 2−7, 19−24.

(Fig. 4A and B). In contrast, Bu8 dissociates more rapidly after block of $Ca_V2.2$, shown by higher recovery ratios of Bu8 (52.6%) compared to MVIIA (42.7%, Fig. 4E). Bu8 also specifically inhibits $Ca_V2.2$, with the inhibitory ratio of 10 μmol/L Bu8 at $Ca_V2.1$ and $Ca_V1.1$ being 27.36 ± 4.48% and 2.82 ± 1.02% (Fig. 5), respectively. Furthermore, 10 μmol/L Bu8 had no significant effect on either voltage-gated sodium or potassium channels in rat DRG neurons (Supporting Information Fig. S32). 10 μmol/L Bu8 also did not impact the function of heterologously expressed $Na_V1.7$ in HEK293 cells (Supporting Information Fig. S33). These results suggest that ω-conotoxin Bu8 selectively inhibits $Ca_V2.2$ channels.

2.5. *Analgesic activity*

The mice hot-plate pain model and acetic acid writhing model were used to assess the analgesic activity of Bu8 and MVIIA. At the three doses (0.33, 1, and 3 μg/kg) tested, Bu8 exhibited potent analgesic activity compared to the saline group in the hot-plate test, and the analgesic activities were similar to MVIIA at all doses tested (Fig. 6). In the acetic acid writhing model, at low and moderate doses (0.33 and 1.0 μg/kg) of Bu8, the writhing numbers of mice was 19.7 ± 4.3 and 10.8 ± 2.6 times, which were significantly lower than that for MVIIA (38.7 ± 3.4 and 32.4 ± 5.7 times) and the saline group (53.4 ± 6.1, 44.3 ± 3.8 times, Fig. 6). These data suggest that Bu8 exhibits higher analgesic activity than MVIIA. At the high dose (3.0 μg/kg), Bu8 (9.7 ± 2.5 times) and MVIIA (10.7 ± 2.3 times) exhibit similar analgesic activity ($P > 0.05$) (Fig. 6). Taken together, these two pain models indicate that Bu8 displays higher or similar analgesic activities than that of MVIIA, particularly at lower doses.

2.6. *Acute toxicity of Bu8 to goldfish*

Goldfish possess a relatively limited blood brain barrier and express some useful behavioral and pharmacologic parallels to the higher vertebrates[32], therefore, they were used to test the toxicity of conotoxins. After intramuscular injections of Bu8 or MVIIA into goldfish (*Carassius carassius*), we observed a dose-dependent behavior of abnormal swimming and mortality (Fig. 7A). MVIIA at 0.4 mg/kg resulted in 100% lethality of goldfish, whereas the same lethality was reached with 0.7 mg/kg Bu8. During a 4 h period, the LD_{50} doses of Bu8 and MVIIA in goldfish are 0.31 (0.22−0.41) mg/kg and 0.21 (0.18−0.24) mg/kg, respectively. These results suggest that Bu8 has lower toxicity than MVIIA.

2.7. *Side effects on the coordinated locomotion in mice*

Typical side-effects of ω-conotoxins are motor disorders and abnormalities in the nervous system, so the effects of Bu8 and

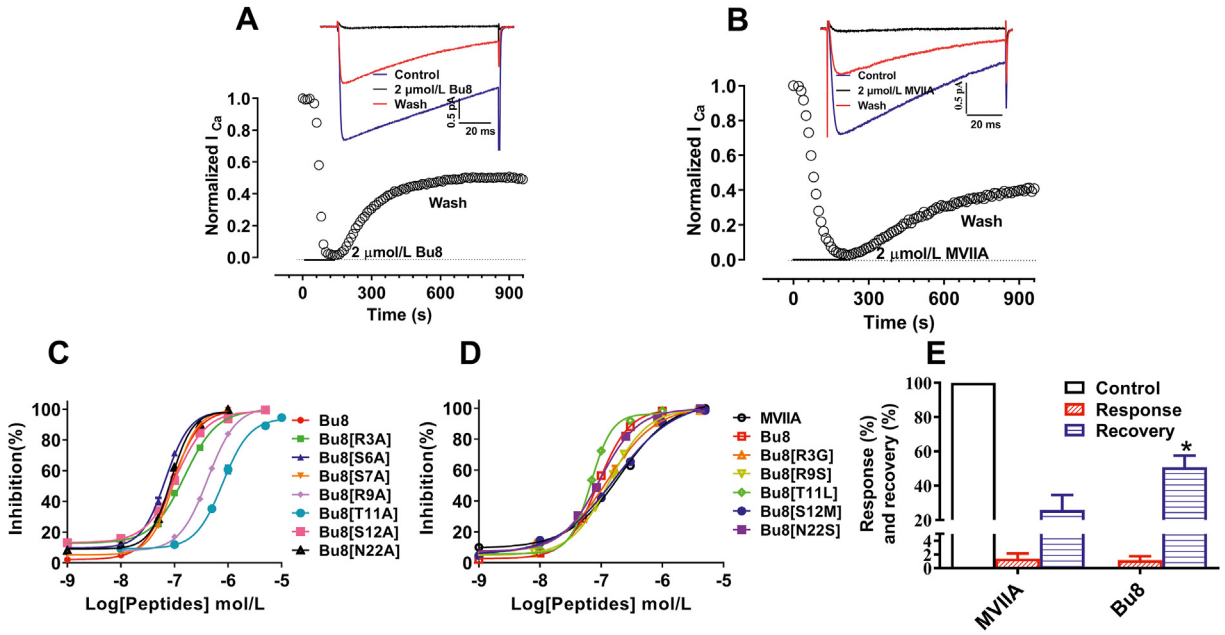

Figure 4 ω-Conotoxins Bu8, MVIIA, and Bu8 mutants inhibited Ba^{2+} currents mediated by $Ca_V2.2$ channels co-expressed with cDNAs encoding α1B, β3 and α2δ subunits in HEK293 cells. (A) and (B) Representative traces of whole-cell currents elicited by a voltage step from a holding potential of −90 mV to a test pulse of +20 mV for 100 ms with a 10 s interval per sweep. The time course of normalized currents of I_{Ca} blocked by Bu8 (A) or MVIIA (B) as indicated. (C) and (D) Concentration−response curves obtained for inhibition of $Ca_V2.2$ by Bu8, MVIIA, and Bu8 mutants. Whole-cell patch clamp recording from HEK293 cells (n = 3−6). (E) The inhibition and recovery ratio obtained for Bu8 and MVIIA at 2 μmol/L ($n > 3$). All data are presented as mean ± SEM.

MVIIA were compared on the coordinated locomotion function 0.5 and 2 h after the administration of three doses of Bu8 and MVIIA. 0.5 h after administration of conotoxins at three different doses, 0.9, 3, and 9 μg/kg, the rotarod times (±SEM) were determined as 125.18 ± 76.91, 39.00 ± 34.85, and 17 ± 18.98 s for Bu8-injected mice, respectively (Fig. 7B and C), which were significantly longer than that of the MVIIA group (32.09 ± 24.94, 9.9 ± 5.4, and 5.64 ± 4.11 s, $P < 0.001$, $P < 0.05$, $P < 0.05$). 2 h after administration, the Bu8 group mice also exhibited significantly longer rotarod times at the low and medium doses (0.9, 3 nmol/kg, $P < 0.05$) but not at a high dose (9 nmol/kg, $P > 0.05$). Overall, Bu8 exhibits lower side effects compared to MVIIA on the coordinated locomotion in mice at similar doses.

3. Discussion

ω-Conotoxin Bu8 potently inhibits $Ca_V2.2$ channels (89 nmol/L) with twice the potency of MVIIA and SO-3. Bu8 also reversibly inhibits $Ca_V2.2$ with high selectivity, its selectivity index for $Ca_V2.1$/$Ca_V2.2$ is at least above 111, since the IC_{50} for $Ca_V2.1$ is <10,000 nmol/L (Fig. 5A). 10 μmol/L of Bu8 also had minimal inhibitory effect on $Ca_V1.1$ channels (Fig. 5B). Bu8 also did not significantly inhibit either voltage-gated sodium or potassium channels in rat DRG neurons or $Na_V1.7$ and $Na_V1.8$ expressed in HEK293T cells (Supporting Information Figs. S32 and S33). These results demonstrate that Bu8 is a selective and reversible $Ca_V2.2$ inhibitor.

The structure−activity relationship of MVIIA showed that Lys2 in loop1 and the residues Ser9, Arg10, Leu11, Met12 and Tyr13 in loop2 are very important for the affinity to $Ca_V2.2$[33,34]. Recently, we found that Lys6 in loop1, Ile11 and Asn14 in loop2 are important functional amino acids for SO-3. Compared to MVIIA[29] and SO-3[30], Bu8 has the same positively charged residues (Lys2, Arg10, Arg21 and Lys24) and Tyr13, so we did not change these residues[31,33−40]. In addition, the amino acid residues in loop3 and loop4 are almost identical. However, Bu8 exhibits the most sequence variety and conformational flexibility in loop 2, in which the hydrophobicity changes greatly because residues 9−12 (Arg-Arg-Thr-Ser) of Bu8 are highly hydrophilic compared to the residues at the corresponding position of MVIIA (Ser-Arg-Leu-Met) and SO-3 (Ser-Arg-Ile-Ala). The backbone alignments among these three peptides shown in Fig. 3C, suggests a less defined folding of Bu8 in the region of loop2 and part of loop3.

CD spectra of the Bu8/MVIIA hybrid T11L and R9S reveal a significant conformational change of the hybrid mutants compared with Bu8 (Fig. 2). Furthermore, the structure−activity relationship analyses reveal that Arg9 and Thr11 are key functional amino acid residues of Bu8, and Bu8/MVIIA hybrid mutants (Arg9/Ser9 or Leu11/Thr11) have lower inhibitory activities compared to Bu8. These results suggest that the binding mode of $Ca_V2.2$ with Bu8 amino acids in loop2 may be different from that of MVIIA, otherwise Bu8 could not be two-fold more potent than MVIIA. The change of global conformation and charges could be the reason of the different binding mode and the increased potency of Bu8. Based on the structure−activity relationships of MVIA, SO-3 and Bu8, we propose that there are two effective pharmacophores in loop2 of ω-conotoxins for their inhibitory activity at $Ca_V2.2$ channels, one is "R(K)RTSYD", and the other is "SR(K)IM(A)YD(N)". Naturally, some amino acid residues in loop1, loop3 and loop4 are also important for the binding or structure stability, such as Lys2 and Arg21[33].

The hot-plate pain model and acetic acid writhing model demonstrate that Bu8 possesses higher or similar analgesic activities compared to MVIIA (Fig. 6), while also exhibiting lower side effects than MVIIA in the coordinated locomotion and

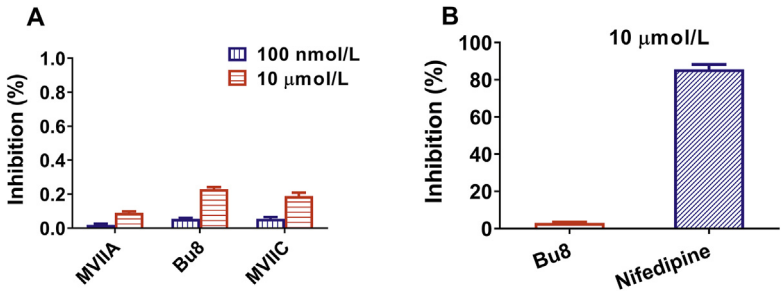

Figure 5 Effect of Bu8, MVIIA and MVIIC on $Ca_V2.1$ and $Ca_V1.1$. $Ca_V2.1$ currents were recorded using the same protocol as $Ca_V2.2$ (Fig. 4), $Ca_V1.1$ currents were recorded with a holding potential of −90 mV stepped to +20 mV. (A) $Ca_V2.1$, the concentration of peptide is 100 nmol/L and 10 μmol/L; (B) $Ca_V1.1$, the concentration of Bu8 and nifedipine is 10 μmol/L. $n = 4–5$. All data are presented as mean ± SEM.

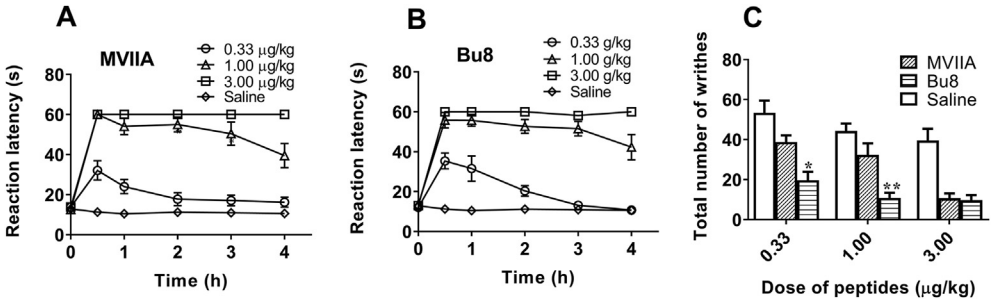

Figure 6 Analgesic activities of Bu8 in (A) and (B) mice hot plate pain model and (C) acetic acid writhing model. The pain threshold of mice was measured after the administration of (A) MVIIA (0.33, 1, and 3 μg/kg, icv) or (B) Bu8 (0.33, 1, and 3 μg/kg, icv) or saline (icv). (C) 20 min after the single administration of MVIIA (0.33, 1 and 3 μg/kg, icv) or Bu8 (0.33, 1 and 3 μg/kg, icv) or saline (icv), acetic acid was administrated (i.p.) and the writhing number of mice was immediately counted for 5 min. Data were expressed as mean ± SEM ($n = 12$). *$P < 0.5$ and **$P < 0.01$ *vs*. the MVIIA group at the same dose. All data are presented as mean ± SEM.

goldfish toxicity experiments (Fig. 7). Because the ratio of IC_{50} ($Ca_V2.2$) to inhibitory rate of Bu8 (100 nmol/L or 10 μmol/L ($Ca_V2.1$)) is slightly higher than that of MVIIA (Fig. 5), its lower side effects is not from the inhibition to $Ca_V2.1$, which is usually considered as a source of side-effects for calcium channel inhibitors. The results of degradation by trysin demonstrate that Bu8 is enzymolysed slightly faster than that of MVIIA (Supporting Information Fig. S34), suggesting that its relatively faster pharmacokinetics in mice may contribute to its lower side-effects, but this may not be the main reason since Bu8 showed higher and similar analgesic activity in 4h. The lower side effects of Bu8 is most likely due to its faster binding and dissociation as well as the higher recovery ratios (52.6%) compared to MVIIA (42.7%, Fig. 4E).

In summary, Bu8 is a potent and selective inhibitor of $Ca_V2.2$ and exhibits potent analgesic activity to acute pain and inflammatory pain. The binding and blocking of $Ca_V2.2$ by Bu8 provide a new clue to designing $Ca_V2.2$ inhibitors with high potency and reduced side effects.

4. Experimental

4.1. Chemicals and biological reagents

N-Fmoc-amino acids, DCC, HOBt, HBTU and TFA were purchased from GL Biochem Ltd. (Shanghai, China). Rink resin was obtained from Tianjin Nankai Hecheng S&T Company. Dithiothreitol (DTT), cysteine, glutathione (GSH) and oxidized glutathione (GSSG) were obtained from Gibco (Carlsbad, CA, USA). Other chemical reagents were of analytical grade. The plasmids of $Ca_V2.2$ ($\alpha1_B$), $Ca_V2.1$ ($\alpha1_A$), $\alpha2\delta$ and $\beta3$ subunits were obtained from Addgene and deposited by Dr. Diane Lipscombe.

4.2. Animals

Kunming mice (18–22 g, 3–4 week old) were obtained from Beijing Animal Center, China, and housed at 23 ± 2 °C with a relative humidity of 50% under a 12 h light/dark cycle. Food pellets and water were available *ad libitum*. All experiments were conducted in accordance with the guidelines of Animal Research Advisory Committee in Beijing Institutes for Biological Science and conformed to the European Community directives for the care and use of laboratory animals.

4.3. Peptide synthesis

The protected Bu8 and its variants were synthesized on Rink resin described previously using an automatic peptide synthesizer (Sophas P-1, Zinsser analytic, Germany) on a 0.1 mmol scale[27,41]. They are cleaved in the mixed solution (8.8 mL trifluoroacetic acid (TFA), 0.5 mL water, 0.5 g DTT, 0.2 mL triisopropylsilane) at room temperature for 3 h. After precipitation with cold diethyl ether (150 mL), the crude peptide (0.2 mg/mL) was oxidized in 0.5 mol/L NH_4Ac buffer (pH 8.0) containing redox agents (1 mmol/L GSH, 0.1 mmol/L GSSG, 1 mmol/L EDTA) at 4 °C. The aim products were then concentrated and purified by semi-preparative RP-HPLC (Waters 1525, USA) using a C18

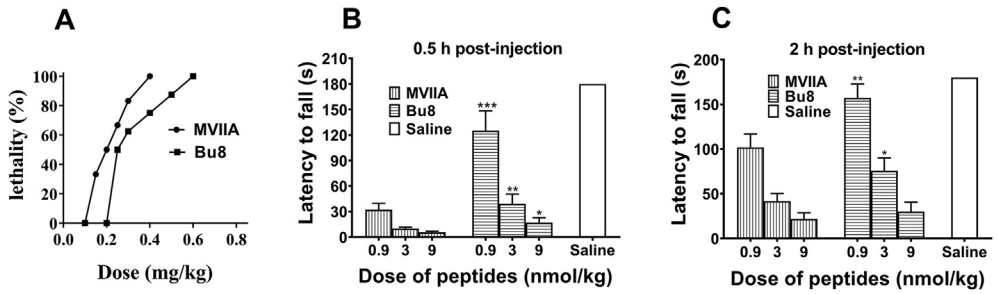

Figure 7 Toxicity of Bu8 on goldfish and mice coordinated locomotion. (A) Dose−response curves of Bu8 and MVIIA in goldfish. The LD_{50} was analyzed by SPSS statistics software version 17.0 (Bliss) within a 4 h period of observation. Ten goldfish were used per dose level. (B) and (C) Effects of Bu8 and MVIIA on coordinated locomotion in the rotarod test. 30 min (B) or 120 min (C) after the injection of each peptide (0.9, 3.0, 9.0 μg/kg, i.c.) or saline intracerebral injection (icv), mice were placed on the rotarod and the staying time was recorded (Section Experimental). Data are presented as mean ± SEM ($n = 10$). *$P < 0.05$, **$P < 0.01$, ***$P < 0.01$ *vs*. MVIIA at the same dose. All data are presented as mean ± SEM.

reversed-phase column (Kromasil, 250 mm × 10.0 mm, 100 Å, 10 μm). The purity of freeze-dried peptides was assessed using the Agilent analytical HPLC (1200 Series, Eclipse Plus C18, 250 mm × 4.6 mm, 100 Å, 5 μm). The primary sequences of Bu8 and its variants are listed in Table 1.

4.4. *Circular dichroism (CD) spectra*

CD spectra were measured using a BioLogic Mos 450 spectropolarimeter (Grenoble, France) as described previously[41]. 35 μmol/L peptide in 0.01 mol/L phosphate buffer (pH 7.2) was added into a 0.1 cm path length quartz cell, three individual scans (190−340 nm) were performed at 1.0 nm intervals with a bandwidth of 1.0 nm.

4.5. *NMR spectroscopy*

Samples of Bu8 were dissolved in 90% H_2O/10% D_2O with 50 mmol/L sodium phosphate at pH 3.5−4.0. ^{1}H-NMR and 2D-NMR spectroscopy including NOESY, TOCSY and DQF-COSY were recorded at 293K on a Bruker AVANCE III 850 MHz spectrometer using TXI cryoprobe[29,42,43]. TOCSY spectra were obtained using the mixing times of 40 and 80 ms. NOESY spectra were determined with mixing times of 100, 200, 300, 400 and 750 ms, respectively. Spectra were processed using NMRPipe and peak analyses were conducted in CARA 1.8.4.2. NOE intensities of NOESY cross peaks were measured by CARA and converted into distance constraints. 76 intra-residue distances, 76 sequential distances, 27 non-sequential distances and 9 disulfide bond constraints were used in the final calculations in accordance with other ω-conotoxins. 200 structures were generated with the simulated annealing algorithm of program Cyana, and 20 lowest-energy states were chosen. Energy minimization were performed using program CNS4. Structure validation was performed on the website PSVS5-6. The data of chemical shifts and spectra were submitted to the BMRB database (ID: 36177) and the PDB database (ID: 5ZNU).

4.6. *Electrophysiological recording from HEK293T cells expressing Ca^{2+} ion channels*

To assess the effects of Bu8 and its variants on $Ca_V2.2$ channels, whole-cell currents through Ca^{2+} channels were recorded using perforated patch recording methods[27,44]. HEK 293 cells were co-transfected with a total of 2 μg of rat $Ca_V2.2$ (α1B), α2δ, β3 subunits and EGFP (the report gene) at a molar ratio of 1:1:1:0.6 for 4 h. 24 h after transfection, whole-cell patch clamp recordings were performed using an Axoclamp 700B patch clamp amplifier (Molecular Devices) at room temperature (~22 °C). The extracellular solution contained: 135 mmol/L *N*-methyl-D-glucamine (NMDG), 20 mmol/L $BaCl_2 \cdot 2H_2O$, 2 mmol/L $MgCl_2 \cdot 2H_2O$ and 10 mmol/L HEPES (pH 7.2). The pipette electrodes had a final resistance of 4−6 MΩ, with an intracellular solution containing (mmol/L): 140 CsCl, 10 NaCl, 1 EGTA and 10 HEPES (pH adjusted to 7.3 with CsOH). $Ca_V2.1$ currents were recorded using the same method as $Ca_V2.2$, but the $Ca_V1.1$ currents were recorded with a holding potential of −90 mV stepped to +20 mV. All data were presented as means ± stand error (SEM) ($n = 3-6$). Half-maximal inhibitory concentrations (IC_{50}s) were obtained from the concentration−response curves of peptide blocking $Ca_V2.2$ currents as described previously[27].

4.7. *Electrophysiological recording of Na^+ and K^+ currents in DRG neurons*

Whole-cell patch-clamp recordings of voltage-gated Na and K^+ currents of DRG neurons were performed as described previously[45,46], the experimental details were described in Supporting Information.

4.8. *Electrophysiological recording of $Na_V1.7$ and $Na_V1.8$ expressed in HEK293 cells*

Electrophysiological recordings of $Na_V1.7$ and $Na_V1.8$ expressed in HEK293 cells were performed as described previously[47]. HEK293 cells transferred with $Na_V1.7$ or $Na_V1.8$ plasmid together with EGFP plasmid and electrophysiological recording conditions were described in Supporting Information.

4.9. *Hot plate test*

The hot plate test was used to assess the analgesic effects of the peptides on female Kunming mice as described previously[25,26,48]. The qualified mice (7 s <pain threshold <18 s) were randomly divided into toxin groups and a saline group, each group contained twelve animals. Pain threshold (reaction latency) on a hot plate (55 ± 0.1 °C) was recorded at 0.5, 1, 2, 3 and 4 h, respectively,

after intracerebral injection (icv) of peptide (10 μL, 0.33, 1 and 3 μg/kg) or saline (10 μL).

4.10. Acetic acid writhing test

Male mice were randomly divided into nine groups including three Bu8 groups, three MVIIA groups and three saline groups. The dose of Bu8 or MVIIA was 0.33, 1 or 3 μg/kg (icv), and the injection volume of saline was 10 μL (icv). 20 min after the toxin or saline administration, 0.4 mL of 1% (*v*/*v*) acetic acid was intraperitoneally injected into each mouse. After 5 min, the number of abdominal contortions (writhes) was recorded during a 15 min period[49,50].

4.11. Toxicity of Bu8 to goldfish

The toxicity of Bu8 and MVIIA to goldfish was determined according to previously reported method[27,32]. Goldfishes (*C. Carassius*, 2.0 ± 0.2 g, one year old, Xingshen fishing ground, Beijing, China) were randomly divided into Bu8 and MVIIA groups with ten goldfishes in each group. Different dose of peptides was injected intramuscularly (6 μL/fish) into goldfish. 4 h after administration of peptide, the number of deaths was recorded and the medium lethal dose (LD_{50}) was analyzed using the SPSS statistics software version 17.0 (Bliss).

4.12. Coordinated locomotion in rotarod test

Motor impairment was determined on the rotating rod (YSL-4C rotarod fatigue apparatus, Academy of Medical Science of Sandong Province, China)[26,50]. 30 and 120 min after the administration (icv) of toxin (10 μL, 0.9, 3.0 and 9 nmol/kg) or saline (10 μL), the half female and half male mice ($n = 10$) were then placed on the rotating rod at a speed of 5 rpm. After 68 s, the rod was accelerated from 5 to 30 rpm over a 3 min interval. The time during which the mice remained balanced on the rod was recorded (3 min as the maximum time).

4.13. Data analysis

The results of analgesic tests were analyzed using one-way ANOVA, followed by student-Newman-keuls test with GraphGad prism 5 (GraphPad Software, La Jolla, CA, USA). All data are presented as mean ± SEM. A P value less than 0.05 was considered statistically significant.

Acknowledgments

This work was financially supported by the National Natural Science Foundation of China (grant number 81473192) and the National Basic Research Program of China (grant number 2010CB529802). We thank Prof David J. Adams, University of Wollongong, for his helpful and insightful comments on the manuscript.

Author contributions

Jinqin Chen, Xinhong Liu and Shuo Yu contributed equally to this work. Jinqin Chen, Shuo Yu, Jia Liu and Rongfang Chen synthesized peptides, performed electrophysiological experiments and determined analgesic activities. Xinhong Liu and Ling Jiang determined the NMR structure and wrote the results. Yunxiao Zhang determined the inhibitory activities to ion channels except calcium ion channel. Qiuyun Dai designed the project and wrote the manuscript.

Conflicts of interest

The authors state no conflicts of interest.

Appendix A. Supporting information

Supporting information to this article can be found online at https://doi.org/10.1016/j.apsb.2021.03.001.

References

1. Mir R, Karim S, Kamal MA, Wilson CM, Mirza Z. Conotoxins: structure, therapeutic potential and pharmacological applications. *Curr Pharm Des* 2016;**22**:582−9.
2. Jin AH, Muttenthaler M, Dutertre S, Himaya S, Kaas Q, Craik DJ, et al. Conotoxins: chemistry and biology. *Chem Rev* 2019;**119**:11510−49.
3. Lewis RJ, Dutertre S, Vetter I, Christie MJ. Conus venom peptide pharmacology. *Pharmacol Rev* 2012;**64**:259−98.
4. Tosti E, Boni R, Gallo A. μ-Conotoxins modulating sodium currents in pain perception and transmission: a therapeutic potential. *Mar Drugs* 2017;**15**:295.
5. Adams DJ, Berecki G. Mechanisms of conotoxin inhibition of N-type ($Ca_V2.2$) calcium channels. *Biochim Biophys* 2013;**1828**:1619−28.
6. Prorok M, Castellino FJ. The molecular basis of conantokin antagonism of NMDA receptor function. *Curr Drug Targets* 2007;**8**:633−42.
7. Pallaghy PK, Nielsen KJ, Craik DJ, Norton RS. A common structural motif incorporating a cystine knot and a triple-stranded beta-sheet in toxic and inhibitory polypeptides. *Protein Sci* 1994;**3**:1833−9.
8. Olivera BM, McIntosh JM, Cruz LJ, Luque FA, Gray WR. Purification and sequence of a presynaptic peptide toxin from *Conus geographus* venom. *Biochemistry* 1984;**23**:5087−90.
9. Olivera BM, Gray WR, Zeikus R, Mclntosh JM, Varga J, Rivier J, et al. Peptide neurotoxins from fish-hunting cone snails. *Science* 1985;**230**:1338−43.
10. Olivera BM, Cruz LJ, de Santos V, LeCheminant GW, Griffin D, Zeikus R, et al. Neuronal calcium channel antagonists. Discrimination between calcium channel subtypes using ω-conotoxin from *Conus magus* venom. *Biochemistry* 1987;**26**:2086−90.
11. Hillyard DR, Monje VD, Mintz IM, Bean BP, Nadasdi L, Ramachandran J, et al. A new *Conus* peptide ligand for mammalian presynaptic Ca^{2+} channels. *Neuron* 1992;**9**:69−77.
12. Ramilo CA, Zafaralla GC, Nadasdi L, Hammerland LG, Yoshikami D, Gray WR, et al. Novel alpha- and omega-conotoxins from *Conus striatus* venom. *Biochemistry* 1992;**31**:9919−26.
13. Woppmann A, Ramachandran J, Miljanich GP. Calcium channel subtypes in rat brain: biochemical characterization of the high-affinity receptors for omega-conopeptides SNX-230 (synthetic MVIIC), SNX-183 (SVIB), and SNX-111(MVIIA). *Mol Cell Neurosci* 1994;**5**:350−7.
14. Fainzilber M, Lodder JC, van der Schors RC, Li KW, Yu Z, Burlingame AL, et al. A novel hydrophobic ω-conotoxin blocks molluscan dihydropyridine-sensitive calcium channels. *Biochemistry* 1996;**35**:8748−52.
15. Lewis RJ, Nielsen KJ, Craik DJ, Loughnan ML, Adams DA, Sharpe IA, et al. Novel ω-conotoxins from *Conus catus* discriminate among neuronal calcium channel subtypes. *J Biol Chem* 2000;**275**:35335−44.
16. Favreau P, Gilles N, Lamthanh H, Bournaud R, Shimahara T, Bouet F, et al. A new ω-conotoxin that targets N-type voltage-sensitive calcium channels with unusual specificity. *Biochemistry* 2001;**40**:14567−75.

17. Wen L, Yang S, Qiao H, Liu Z, Zhou W, Zhang Y, et al. SO-3, a new *O*-superfamily conopeptide derived from *Conus striatus*, selectively inhibits N-type calcium currents in cultured hippocampal neurons. *Br J Pharmacol* 2005;**145**:728−39.
18. Berecki G, Motin L, Haythornthwaite A, Vink S, Bansal P, Drinkwater R, et al. Analgesic ω-conotoxins CVIE and CVIF selectively and voltage-dependently block recombinant and native N-type calcium channels. *Mol Pharmacol* 2010;**77**:139−48.
19. Lee S, Kim Y, Back SK, Choi HW, Lee JY, Jung HH, et al. Analgesic effect of highly reversible ω-conotoxin FVIA on N type Ca^{2+} channels. *Mol Pain* 2010;**6**:97.
20. Bernáldez J, Román-González SA, Martínez O, Jiménez S, Vivas O, Arenas I, et al. A *Conus regularis* conotoxin with a novel eight-cysteine framework inhibits $Ca_V2.2$ channels and displays an antinociceptive activity. *Mar Drugs* 2013;**11**:1188−202.
21. Sousa SR, McArthur JR, Brust A, Bhola RF, Rosengren KJ, Ragnarsson L, et al. Novel analgesic ω-conotoxins from the vermivorous cone snail *Conus moncuri* provide new insights into the evolution of conopeptides. *Sci Rep* 2018;**8**:13397.
22. Jurkovicova-Tarabova B, Lacinova L. Structure, function and regulation of $Ca_V2.2$ N-type calcium channels. *Gen Physiol Biophys* 2019;**38**:101−10.
23. Patel R, Montagut-Bordas C, Dickenson AH. Calcium channel modulation as a target in chronic pain control. *Br J Pharmacol* 2018;**175**:2173−84.
24. Cui C, Merritt R, Fu L, Pan Z. Targeting calcium signaling in cancer therapy. *Acta Pharm Sin B* 2017;**7**:3−17.
25. Deer TR, Pope JE, Hanes MC, McDowell GC. Intrathecal therapy for chronic pain: a review of morphine and ziconotide as first line options. *Pain Med* 2019;**20**:784−98.
26. Dai QY, Liu FY, Zhou YR, Lu BS, Yu F, Huang PT. The synthesis of SO-3, a conopeptide with high analgesic activity derived from *Conus striatus*. *J Nat Prod* 2003;**66**:1276−9.
27. Wang F, Yan Z, Liu Z, Wang S, Wu Q, Yu S, et al. Molecular basis of toxicity of N-type calcium channel inhibitor MVIIA. *Neuropharmacology* 2016;**101**:137−45.
28. Hao H, Bandyopadhyay PK, Olivera BM, Yandell M. Characterization of the *Conus bullatus* genome and its venom-duct transcriptome. *BMC Genom* 2011;**12**:60.
29. Kohno T, Kim JI, Kobayashi K, Kodera Y, Maeda T, Sato K. Three-dimensional structure in solution of the calcium channel blocker omega-conotoxin MVIIA. *Biochemistry* 1995;**34**:10256−65.
30. Yan YB, Tu GZ, Luo XC, Dai QY, Huang PT, Zhang RQ. Three-dimensional solution structure of ω-conotoxin SO-3 determined by ^{1}HNMR. *Chin Sci Bull* 2003;**48**:1097−102.
31. Kim JI, Takahashi M, Ohtake A, Wakamiya A, Sato K. Tyr13 is essential for the activity of omega-conotoxin MVIIA and GVIA, specific N-type calcium channel blockers. *Biochem Biophys Res Commun* 1995;**206**:449−54.
32. Adeyemo OM, Shapira S, Tombaccini D, Pollard HB, Feuerstein G, Siren AL. A goldfish model for evaluation of the neurotoxicity of ω-conotoxin GVIA and screening of monoclonal antibodies. *Toxicol Appl Pharmacol* 1991;**108**:489−96.
33. Nielsen KJ, Adams D, Thomas L, Bond T, Alewood PF, Craik DJ, et al. Structure–activity relationships of ω-conotoxins MVIIA, MVIIC and 14 loop splice hybrids at N and P/Q-type calcium channels. *J Mol Biol* 1999;**289**:1405−21.
34. Nielsen KJ, Adams DA, Alewood PF, Lewis RJ, Thomas L, Schroeder T, et al. Effects of chirality at Tyr13 on the structure−activity relationships of ω-conotoxins from *Conus magus*. *Biochemistry* 1999;**38**:6741−51.
35. Flinn JP, Pallaghy PK, Lew MJ, Murphy R, Angus JA, Norton RS. Roles of key functional groups in ω-conotoxin GVIA synthesis, structure and functional assay of selected peptide analogues. *Eur J Biochem* 1999;**262**:447−55.
36. Nielsen KJ, Schroeder T, Lewis R. Structure−activity relationships of ω-conotoxins at N-type voltage-sensitive calcium channels. *J Mol Recognit* 2000;**13**:55−70.
37. Sato K, Raymond C, Martin-Moutot N, Sasaki T, Ohtake A, Minami K, et al. Binding of six chimeric analogs of ω-conotoxin MVIIA and MVIIC to N- and P/Q-type calcium channels. *Biochem Biophys Res Commun* 2000;**269**:254−6.
38. Feng ZP, Doering CJ, Winkfein RJ, Beedle AM, Spafford JD, Zamponi GW. Determinants of inhibition of transiently expressed voltage-gated calcium channels by ω-conotoxins GVIA and MVIIA. *J Biol Chem* 2003;**278**:20171−8.
39. Schroeder CI, Nielsen KJ, Adams DA, Loughnan M, Thomas L, Alewood PF, et al. Effects of Lys2 to Ala2 substitutions on the structure and potency of ω-conotoxins MVIIA and CVID. *Biopolymers* 2012;**98**:345−56.
40. Lee MS. Recent progress in the discovery and development of N-type calcium channel modulators for the treatment of pain. *Prog Med Chem* 2014;**53**:147−86.
41. Cai F, Xu N, Liu Z, Ding R, Yu S, Dong M, et al. Targeting of N-type calcium channels *via* GABAB-receptor activation by α-conotoxin Vc1.1 variants displaying improved analgesic activity. *J Med Chem* 2018;**61**:10198−205.
42. Liu Z, Bartels P, Sadeghi M, Du T, Dai Q, Zhu C, et al. A novel α-conopeptide Eu1.6 inhibits N-type ($Ca_V2.2$) calcium channels and exhibits potent analgesic activity. *Sci Rep* 2018;**8**:1004.
43. Wang S, Du T, Liu Z, Wang S, Wu Y, Ding J, et al. Characterization of a T-superfamily conotoxin TxVC from *Conus textile* that selectively targets neuronal nAChR subtypes. *Biochem Biophys Res Commun* 2014;**454**:151−6.
44. Dong M, Wang F, Yan Z, Yu S, Wei J, Wu Q, et al. Structure−activity analysis of N-type calcium channel inhibitor SO-3. *Biochemistry* 2018;**57**:6349−55.
45. Xiao Z, Zhang Y, Zeng J, Liang S, Tang C, Liu Z. Purification and Characterization of a novel insecticidal toxin, μ-sparatoxin-Hv2, from the venom of the spider *Heteropoda venatoria*. *Toxins (Basel)* 2018;**10**:233.
46. Chen M, Li J, Zhang F, Liu Z. Isolation and characterization of SsmTx-I, a specific Kv2.1 blocker from the venom of the centipede scolopendra subspinipes mutilans L. Koch. *J Pept Sci* 2014;**20**:159−64.
47. Zhou X, Zhang Y, Tang D, Liang S, Chen P, Tang C, et al. A Chimeric $Na_V1.8$ channel expression system based on HEK293T cell line. *Front Pharmacol* 2018;**9**:337.
48. Ren B, Zhou Z, Liu Z, Li B, Ou J, Dai Q. Con-T[M8Q] potently attenuates the expression and development of morphine tolerance in mice. *Neurosci Lett* 2015;**597**:38−42.
49. Yan LD, Liu YL, Zhang L, Dong HJ, Zhou PL, Su RB, et al. Spinal antinociception of synthetic omega-conotoxin SO-3, a selective N-type neuronal voltage-sensitive calcium channel blocker, and its effects on morphine analgesia in chemical stimulus tests in rodent. *Eur J Pharmacol* 2010;**636**:73−81.
50. Malmberg AB, Gilbert H, McCabe RT, Basbaum AI. Powerful antinociceptive effects of the cone snail venom-derived subtype-selective NMDA receptor antagonists conantokins G and T. *Pain* 2003;**101**:109−16.